Minority-carrier lifetime enhancement in edge-defined film-fed grown Si through rapid thermal processing-assisted reduction of hydrogen-defect dissociation

Kenta Nakayashiki[a] and Ajeet Rohatgi
University Center of Excellence for Photovoltaics Research and Education, School of Electrical and Computer Engineering, Georgia Institute of Technology, Atlanta, Georgia 30332

Sergei Ostapenko and Igor Tarasov
Nanomaterials and Nanomanufacturing Research Center, University of South Florida, Tampa, Florida 33620

(Received 12 July 2004; accepted 18 October 2004; published online 23 December 2004)

This paper demonstrates that a very short, 1-s, simultaneous firing of screen-printed Al at the back and SiN_x antireflection (AR) coating at the front can significantly enhance the minority-carrier lifetime in edge-defined film-fed grown (EFG) ribbon Si via SiN_x-induced hydrogen passivation of defects. It was found that 1-s firing in a rapid thermal processing system at an optimum temperature improved the average minority-carrier lifetime from 3 to >80 μs, resulting in $\sim$16% efficient 4-cm^2 screen-printed EFG Si cells. It is proposed that rapid thermal firing enhances the retention of hydrogen at defect sites by minimizing the hydrogen-defect dissociation. A combination of simulations and experiments reveals that the dissociation of hydrogen is extremely rapid at conventional firing temperatures of $\sim$700 °C. An activation energy of 2.4–2.6 eV was determined for the hydrogen-defect dissociation in EFG Si. This activation energy, in conjunction with the room-temperature photoluminescence data, suggests that the impurity-decorated dislocations are the dominant hydrogenation and dehydrogenation sites in the EFG Si. Based on the above understanding, a manufacturable process, involving rapid co-firing of SiN_x AR coating, screen-printed Al-doped back surface field (Al-BSF), and screen-printed Ag front grid, was developed in a conventional belt furnace to minimize the degree of dehydrogenation while producing good Al-BSF and ohmic contacts. This process produced 4-cm^2 screen-printed EFG Si cells with an efficiency of 15.9%. © *2005 American Institute of Physics*. [DOI: 10.1063/1.1833577]

I. INTRODUCTION

Edge-defined film-fed grown (EFG) ribbon Si is a promising candidate for cost-effective photovoltaic (PV) systems because it eliminates the kerf loss and the mechanical sawing process. However, EFG Si suffers from relatively high concentrations of metallic impurities and crystallographic defects, such as dislocations and grain boundaries.[1] These defects lead to a very low as-grown minority-carrier lifetime, typically less than 3 μs, which is not sufficient for producing high-efficiency cells. Therefore, it is necessary to enhance the carrier lifetime during cell processing to reach the full potential of EFG Si for cost-effective PV.

It has been shown that SiN_x-induced hydrogen passivation of defects plays an important role in enhancing the carrier lifetime in ribbon Si.[2–4] Furthermore, simultaneous firing of SiN_x antireflection (AR) coating and screen-printed Al provides an additional driving force for hydrogenation of defects, in addition to forming back contact and an Al-doped back surface field (Al-BSF).[5–7] To realize maximum benefit from a hydrogenation source, it is critical to optimize the firing process to achieve high retention of atomic hydrogen at the defect sites. The implementation of a short firing time in a rapid thermal processing (RTP) system has been shown to produce very high-efficiency ribbon Si solar cells (18.2% on EFG and 17.8% on String Ribbon Si) with photolithography front contacts.[8] Fabrication of these ribbon Si cells involved phosphorus diffusion in a $POCl_3$ furnace to form 85 Ω/sq n^+ emitter, SiN_x AR coating deposition in a low-frequency plasma-enhanced chemical-vapor deposition (PECVD) reactor, Al screen-printing at the back, rapid thermal firing (1 s) at 740–750 °C in a RTP system, photolithography front contact, and SiN_x/MgF_2 double-layer AR coating.

RTP is an attractive tool for solar cell fabrication because it allows excellent control of temperature ramp-up and cooling rates as well as peak-holding interval. RTP has been used successfully in the laboratory for many Si solar cell fabrication steps, such as oxidation for surface passivation, diffusion for shallow emitter formation, and firing for screen-printed contacts.[9–11] Limited data in the literature suggest that RTP provides a better opportunity to control and optimize the firing cycle for enhancing the material properties and device performance.[11] Even though the PV industry currently uses conventional belt-line or tube furnaces for cell fabrication, the development of a continuous RTP machine could improve the throughput and provide a promising alternative for cost-effective and clean processing. This study shows how the use of RTP can improve the defect hydrogenation in EFG Si via controlled rapid firing of screen-printed

[a]Electronic mail: gtg997i@mail.gatech.edu

contacts, resulting in significant enhancement in carrier lifetime and cell performance. The understanding gained from the RTP study is used to develop a co-firing process for front and back screen-printed contacts in a continuous belt furnace to achieve high bulk carrier lifetime and high-efficiency EFG Si solar cells.

II. EXPERIMENT

In this study, simple n^+-p-p^+ EFG Si solar cells are fabricated with screen-printed Al at the back and a screen-printed Ag grid at the front. EFG wafers were provided by RWE Schott Solar, Inc. (Billerica, MA), which is the current leader in production volume of ribbon Si solar cells.[12] Nine 4-cm^2 cells were fabricated on each 100-cm^2 wafer and isolated by a dicing saw. The resistivity of the EFG Si was 3–4 Ω cm, and the cell thickness was $\sim$300 μm. After the initial cleaning process, all the wafers were phosphorus diffused using a $POCl_3$ source in a tube furnace to form 40–50 Ω/sq n^+ emitter. A SiN_x AR coating with a thickness of $\sim$800 Å and a refractive index of 2.0 was deposited in a low-frequency PECVD reactor. A commercial Al paste was screen printed at the back followed by different hydrogenation anneals in a RTP system to find the optimum firing temperature for the 1-s hold time.

It has been suggested in the literature that the release of hydrogen atoms from the remote PECVD SiN_x film is very rapid initially and then slows down.[13] This implies that the hydrogen supply may decrease rapidly with time, while hydrogen dissociation from the passivated defects continues during the holding interval. As a result, a short firing time should be able to retain more hydrogen atoms at the defect sites and produce a higher minority-carrier lifetime. Since the rate of dehydrogenation is also governed by the temperature, the defect hydrogenation anneals were performed in a RTP unit at 725, 750, 775, 800, and 825 °C for 1 s with a fast temperature ramp-up rate of 100 °C/s and a cooling rate of −40 °C/s. The Ag front grid was then screen printed and fired by a second RTP anneal using similar ramp-up and cooling rates. A forming gas contact anneal was performed at 400 °C for 15 min at the end of the process. Thirty six 4-cm^2 cells were fabricated for each process scheme in this study to account for the inhomogeneity in the material quality of the EFG Si. Illuminated current–voltage measurements were performed to extract the cell performance parameters. After establishing the sensitivity of the firing cycle and the optimum firing cycle for the two-step RTP process (the first step for hydrogenation and the second step for Ag contact formation), a single-step belt furnace process was developed in the continuous belt furnace during which SiN_x AR coating, Al-BSF, and Ag grid were fired simultaneously. Finally, EFG Si cells were stripped down to bare Si, and minority-carrier lifetime was measured in each sample at an injection level of 1.0×10^{15} cm^{-3}, using the quasi-steady-state photoconductance (QSSPC) technique to quantify the degree of process-induced hydrogen passivation.[14] In selected cases, hydrogenated bare EFG Si samples were reannealed systematically to study the dehydrogenation kinetics by monitoring the rate of change in minority-carrier lifetime.

TABLE I. Average cell parameters for each firing scheme. Firing time was 1 s for all cases.

(°C)	V_{OC} (mV)	J_{SC} (mA/cm^2)	FF	Eff (%)
725	587	33.8	0.737	14.6
750	589	33.8	0.738	14.7
775	600	33.9	0.748	15.3
800	596	34.0	0.724	14.6
825	579	32.4	0.720	13.5

III. RESULTS AND DISCUSSION

A. Optimization of SiN_x-induced defect hydrogenation in RTP

EFG Si solar cells were initially fabricated by the two-step RTP firing process. The first step involved 1-s hydrogenation at different temperatures, during which SiN_x at the front and Al at the back were fired simultaneously. The second RTP step involved firing the Ag grid after screen printing the Ag paste. Table I shows the average values of the open-circuit voltage (V_{OC}), short-circuit current density (J_{SC}), fill factor (FF), and efficiency for each firing scheme. Table I indicates that firing at 775 °C for 1 s gave a maximum average V_{OC} (600 mV). Average FF decreased from 0.748 to 0.720 when the firing temperature was raised from 775 to 825 °C because the Ag paste used in this experiment produced the best contacts in the range of 750–775 °C for the 1-s firing. Figure 1 shows the average cell efficiency for each scheme as a function of peak hydrogenation temperature. The hydrogenation at 775 °C for 1 s gave the average efficiency of 15.3% with a maximum of 15.9% (V_{OC} = 605 mV, J_{SC} = 34.11 mA/cm^2, FF = 0.769), which was confirmed by the National Renewable Energy Laboratory (Golden, CO). Figure 1 also reveals that hydrogenation at a higher firing temperature ($\geqslant$800 °C) produces less efficient EFG Si solar cells. The average cell efficiency for 825 °C/1 s hydrogenation was only 13.5%, indicating a 1.8% loss in absolute efficiency compared to the 775 °C/1 s hydrogenation. This loss is largely attributed to the carrier

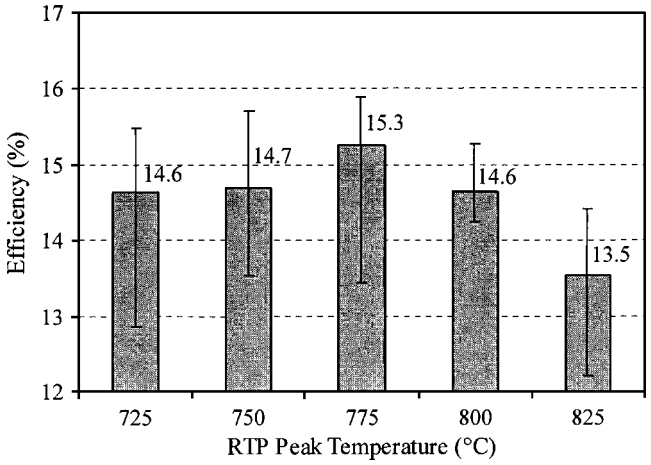

FIG. 1. Efficiencies of EFG Si cells as a function of 1-s firing at peak hydrogenation temperature, followed by Ag contact firing at 700 °C for 1 s.

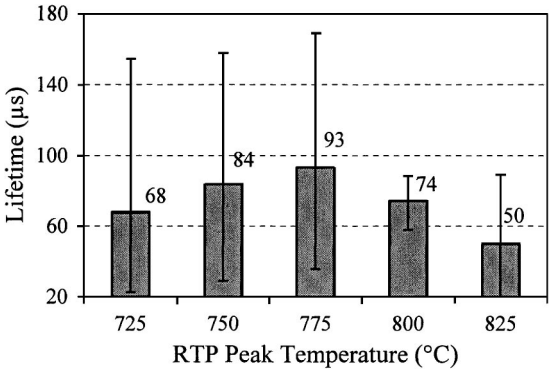

FIG. 2. Average lifetime achieved for each firing scheme in Fig. 1 as a function of peak firing temperature.

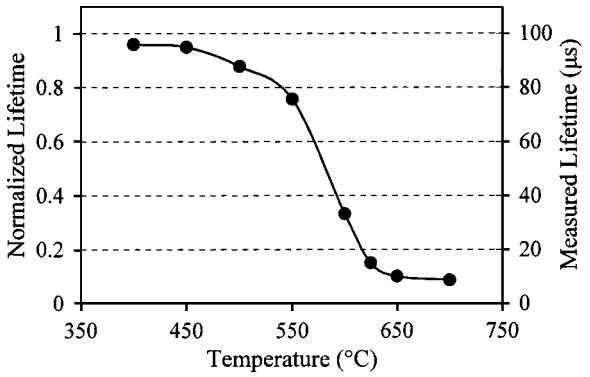

FIG. 3. Normalized lifetime (τ_f/τ_i) as a function of temperature for 1-s annealing of the hydrogenated bare EFG Si sample.

lifetime degradation because of the enhanced dissociation of atomic hydrogen from the hydrogenated-defect sites at higher temperature.

To support the above hypothesis, QSSPC lifetime measurements were performed after stripping the cell down to bare Si. Figure 2 shows that an average minority-carrier lifetime of 93 μs was achieved with a maximum of 169 μs for the peak hydrogenation temperature of 775 °C. It should be noted that the lifetimes were measured by the QSSPC technique and averaged over 32 different locations (four wafers and eight different locations per wafer) on EFG Si for each firing scheme. The average carrier lifetime decreased to 74 μs for the 800 °C/1 s hydrogenation and to 50 μs for the 825 °C/1 s hydrogenation. This decreasing trend in carrier lifetime at higher temperature is consistent with the trend in cell performance in Table I. It is proposed that this decreasing trend in carrier lifetime is the result of reactivation of hydrogenated defects at higher annealing temperature. The degree of hydrogenation is dictated by the competition between the supply of hydrogen atoms to the defects from the SiN_x layer and the dissociation of hydrogen from the defects. These two processes happen simultaneously during the hydrogenation cycle.

B. Understanding and kinetics of the hydrogen-defect dissociation process in EFG Si

To understand and quantify the hydrogen-defect dissociation process, hydrogenated samples (750 °C/1 s firing in RTP) were first etched down to bare Si to remove the hydrogen supply (SiN_x film) and were then reannealed in the RTP unit in the temperature range of 400–700 °C for 1 s. Some samples were also reannealed at 550 °C for 5–60 s to study the reactivation of hydrogenated defects as a function of time at a lower temperature. Float zone (FZ) Si with a resistivity of 1.3 Ω cm was used as a control to ensure that the change in carrier lifetime is primarily due to the hydrogen out diffusion and not because of any contamination during the heat treatment. Figure 3 shows a rapid decrease in carrier lifetime above 550 °C for 1-s anneal, while no appreciable change in carrier lifetime was observed in FZ Si, which remained at 270–300 μs after 700 °C/1 s and 550 °C/60 s RTP annealing. Figure 3 also shows that the normalized lifetime, τ_f/τ_i, where τ_i and τ_f are the carrier lifetimes before and after annealing of hydrogenated samples, respectively, was not affected below 500 °C for the 1-s anneal. However, the carrier lifetime dropped from 99 to 8.3 μs ($\tau_f/\tau_i \simeq 0.08$) after 700 °C/1 s annealing. Figure 4 shows that the carrier lifetime decreases with the increased firing time even at 550 °C. Figures 3 and 4 clearly indicate that the hydrogen-defect dissociation starts to occur even below the conventional contact firing temperatures in the range of 700–800 °C and its effect could become very significant for longer-holding times if the hydrogen supply is cut off or becomes limited.

The hydrogen-defect dissociation can be expressed by the following reaction:

$$XH \xrightarrow{\text{dissociation}} X + H, \tag{1}$$

where H represents hydrogen and X represents a defect or impurity. Assuming that a hydrogen-defect complex (XH) dissociates in accordance with the first-order reaction kinetics, the rate of change in the density of hydrogen-defect complexes, (XH), can be expressed as[15]

$$\frac{d(XH)}{dt} = -k(XH), \tag{2}$$

$$\int_{N_O}^{N} \frac{d(XH)}{(XH)} = \int_0^t -k\,dt, \tag{3}$$

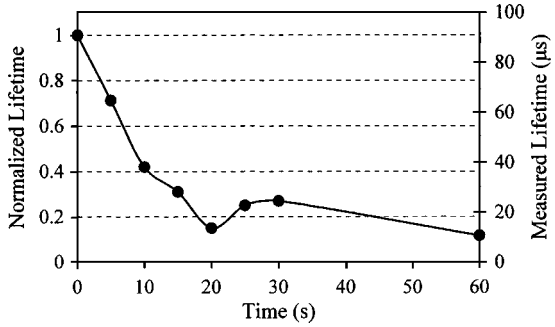

FIG. 4. Normalized lifetime (τ_f/τ_i) of a hydrogenated bare EFG Si sample as a function of annealing time at 550 °C.

$$\ln \frac{N}{N_O} = -kt, \tag{4}$$

where k is the reaction-rate constant, N_O is the density of hydrogen-defect complexes prior to annealing the hydrogenated sample, and N is the density of hydrogen-defect complexes after the heat treatment for time t. Most first-order reactions are characterized by an activation energy, and their rate is often expressed by the Arrhenius equation,

$$k = \nu \exp\left(\frac{-E_D}{k_B T}\right), \tag{5}$$

where υ is the frequency factor (frequency of dissociation attempts), E_D is the activation energy, k_B is the Boltzmann constant, and T is the temperature.[15] Substituting Eq. (5) into Eq. (4) gives

$$\ln \frac{N}{N_O} = -t\nu \exp\left(\frac{-E_D}{k_B T}\right) \tag{6}$$

or

$$\frac{N}{N_O} = \exp\left[-t\nu \exp\left(\frac{-E_D}{k_B T}\right)\right], \tag{7}$$

where N/N_O is the fraction of passivated defects (hydrogen-defect complexes) remaining after a dehydrogenation anneal.[16–20]

Since it is difficult to measure N_O and N directly, Eq. (7) was transformed in terms of measured lifetimes τ_i and τ_f, assuming that τ at any stage is inversely proportional to the concentration of unpassivated active defects. The fraction of passivated defects (hydrogen-defect complexes), N/N_O, can now be written as

$$\frac{N}{N_O} = \frac{\text{concentration of passivated defects after annealing}}{\text{concentration of passivated defects before annealing}} = \frac{N_T - N'}{N_T - N'_O}, \tag{8}$$

where N'_O and N' are the concentrations of unpassivated defects before and after annealing, respectively, which dictate the carrier lifetime. Note that N'_O and N' are inversely proportional to τ_i and τ_f, respectively. N_T is the total concentration of lifetime-limiting defects that can be passivated, which is also equal to the unpassivated defect concentration when all the hydrogenated defects are reactivated and the lifetime does not decrease with further annealing. The fraction of passivated defects can now be expressed in terms of measured carrier lifetimes,

$$\frac{N}{N_O} = \frac{1/\tau_s - 1/\tau_f}{1/\tau_s - 1/\tau_i}, \tag{9}$$

where τ_s is the saturated lifetime when all the hydrogenated defects are reactivated and the lifetime does not decrease with further annealing. In this study, the fully dehydrogenated carrier lifetime, τ_s, is 8 μs, which is obtained after annealing the samples at 700 °C for 60 s. τ_i is 99 μs for the temperature-dependence study in Fig. 3 and 91 μs for the time-dependence study in Fig. 4. According to the literature,

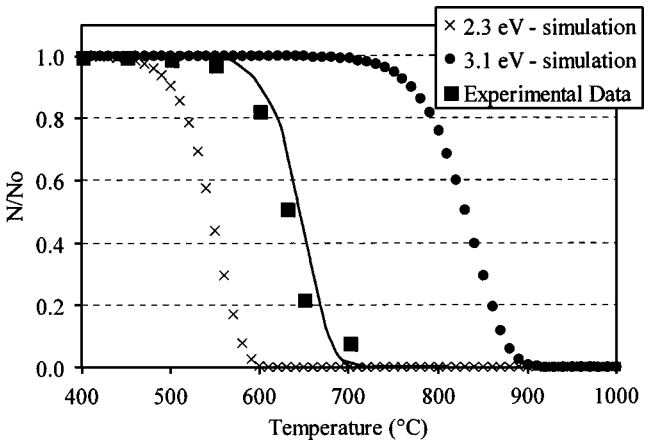

FIG. 5. A comparison of simulation and experimental data showing a fraction of passivated defect as a function of annealing temperature for 1-s annealing of a hydrogenated bare EFG Si sample ($\nu = 1.0 \times 10^{14}$).

the attempt dissociation frequency, ν, falls in the range of 1.0×10^{13} to 10^{14} s^{-1} and was set to 1.0×10^{14} s^{-1} for the model calculations shown in Figs. 5 and 6 using Eq. (7).[17,18]

Figures 5 and 6 show the comparison between the experimental data and model calculations. Simulations were performed using Eq. (7). Figure 5 shows the case for 1-s dehydrogenation at different temperatures, and Fig. 6 shows the case of annealing at 550 °C for different times. Based on the limited data in the literature, the E_D values fall in the range of 1.5–2.5 eV for hydrogen-impurity complex dissociation, and its value is 3.1 eV for hydrogen-dislocation complex dissociation.[18,19] Two curves were first simulated and plotted on Figs. 5 and 6 using Eq. (7) and E_D values of 2.3 and 3.1 eV to cover the range of hydrogen dissociation from impurities and dislocations. The measured carrier lifetime data were then used to calculate N/N_O according to Eq. (9) and plotted on Figs. 5 and 6 with the simulated curves. Notice that the experimental data fall within the simulated curves for the hydrogen-impurity and hydrogen-dislocation dissociation in both figures. This supports the dehydrogenation or reactivation of passivated impurities, dislocations, or impurity-decorated dislocations during the annealing pro-

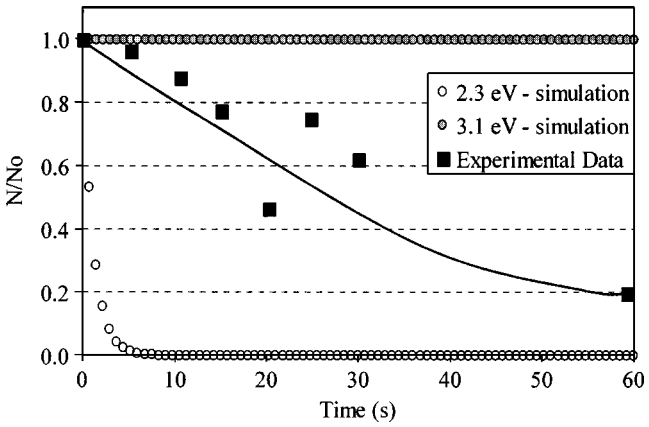

FIG. 6. A comparison of simulation and experimental data showing a fraction of passivated defect in a hydrogenated EFG Si sample as a function of annealing time at 550 °C ($\nu = 1.0 \times 10^{14}$).

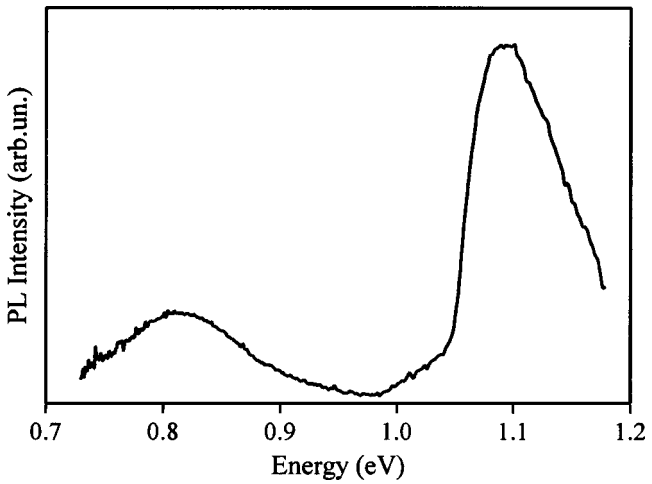

FIG. 7. Room-temperature PL spectra on EFG Si after RTP dehydrogenation at 600 °C/1 s.

cess. The model fitted to the experimental data gave an activation energy E_D of 2.4 eV for ν of 1.0×10^{13} s^{-1} and 2.6 eV for ν of 1.0×10^{14} s^{-1} in EFG Si.

C. Scanning photoluminescence mapping to study the hydrogen passivation and reactivation of defects in EFG Si

After determining the activation energy for the hydrogen-defect dissociation, room-temperature scanning photoluminescence (PL) spectroscopy was performed in an attempt to identify the nature of the passivated defects and to understand the process of hydrogen dissociation from the electrically active defects in EFG Si. The PL spectrum was taken at room temperature using AlGaAs laser excitation. Figure 7 shows two peaks in the PL spectra: one at 0.8 eV corresponding to the defect band with PL intensity of I_{def} and the other at 1.1 eV corresponding to the band-to-band PL intensity of I_{bb}. It has been shown in Refs. 21 and 22 that the defect band peak at 0.8 eV corresponds to impurity-decorated dislocations, which supports the conclusion from the activation energy analysis in Sec. III B. PL mappings were performed on a 50×22-mm^2 EFG Si piece with a spatial resolution of 0.5 mm. The EFG Si samples were cleaned and phosphorus diffused, coated with SiN_x in a low-frequency PECVD reactor, and hydrogenated in a RTP unit at 750 °C for 1 s. The SiN_x AR coating was then removed in 10:1 H_2O:HF solution prior to the PL measurements.

The intensity of both bands, I_{bb} and I_{def}, at a constant generation rate, G, can be expressed in terms of effective minority-carrier lifetime (τ_{eff}), radiative band-to-band recombination lifetime (τ_{rad}), and radiative component of Shockley–Read–Hall lifetime (τ_{SRH}). The τ_{eff} is the composite of radiative, nonradiative, and surface recombinations and is generally dominated by nonradiative recombination in Si.[21]

$$I_{bb} = C_1 G \frac{\tau_{eff}}{\tau_{rad}}, \tag{10}$$

TABLE II. Average values of PL intensities for I_{bb}, I_{def}, and R parameter in each step.

	Initial	Hydrogenated	600 °C/1 s dehydrogenated	700 °C/1 s dehydrogenated
I_{bb}	28.81	126.33	112.47	42.80
I_{def}	n.a.[a]	0.708	0.613	0.339
R parameter	n.a.[a]	0.0111	0.0127	0.0237

[a]PL intensity is below sensitivity limit.

$$I_{def} = C_2 G \frac{\tau_{eff}}{\tau_{SRH}}, \tag{11}$$

$$\tau_{SRH} = (N_{def} v_{th} \sigma_n)^{-1}, \tag{12}$$

where C_1 and C_2 are the temperature-dependent Si constants, N_{def} is the concentration of radiative defect centers, v_{th} is the electron thermal velocity, and σ_n is the electron-capture cross section of radiative centers.[21,22] Equation (10) shows that the I_{bb} is proportional to the effective minority-carrier lifetime, τ_{eff}, since τ_{rad} is a constant for a given resistivity of Si. Thus, PL mapping of the EFG Si wafer will reveal the regions of good lifetime as high I_{bb}. According to Eq. (11), I_{def} is inversely proportional to the radiative component of the Shockley–Read–Hall lifetime. I_{def} is localized in low lifetime regions and generally gives nearly inverse contrast with I_{bb} and effective lifetime maps.[21] The point-by-point ratio of the two PL intensities gives R (R parameter), which is proportional to the concentration of radiative defects at a given illumination intensity. R is expressed by the following equation:

$$R = I_{def}/I_{bb} = \text{const} \times N_{def}. \tag{13}$$

R is independent of other recombination channels in the bulk and at the surface.

Table II summarizes the two PL intensities and R parameter after 750 °C/1 s hydrogenation and 600 °C/1 s and 700 °C/1 s dehydrogenation processes. I_{bb}, which is proportional to the effective carrier lifetime, increased from 29 to 126 (arbitrary unit) after 750 °C/1 s RTP hydrogenation. The I_{bb} decreased from 126 to 42 after the subsequent 700 °C/1 s dehydrogenation step. A substantial reduction in I_{bb} supports the rapid dissociation of hydrogen from defect sites at 700 °C, which was also observed experimentally in Sec. III B.

Figure 8 shows the PL maps of (a) I_{bb}, (b) I_{def}, and (c) point-by-point ratio of I_{bb} [I_{bb}(hydrogenated)/I_{bb}(initial)] for the EFG Si sample. Figure 9 shows the results of a line scan through the above sample at a specific location to assess spatial variation in the reduction in the carrier lifetime [I_{bb}(dehydrogenated)/I_{bb}(hydrogenated)] after 700 °C/1 s dehydrogenation and the radiative defect concentration, R, after 750 °C/1 s hydrogenation and 700 °C/1 s hydrogenation and 700 °C/1 s dehydrogenation. Figure 8 shows the inverse contrast between I_{bb} and I_{def}. It is clear from Figs. 8 and 9 that highly defective regions (low I_{bb} and high R) show much greater reduction in the effective lifetime after the 700 °C/1 s dehydrogenation. Figure 9 shows that in the low effective lifetime region, the impurity-decorated dislocations

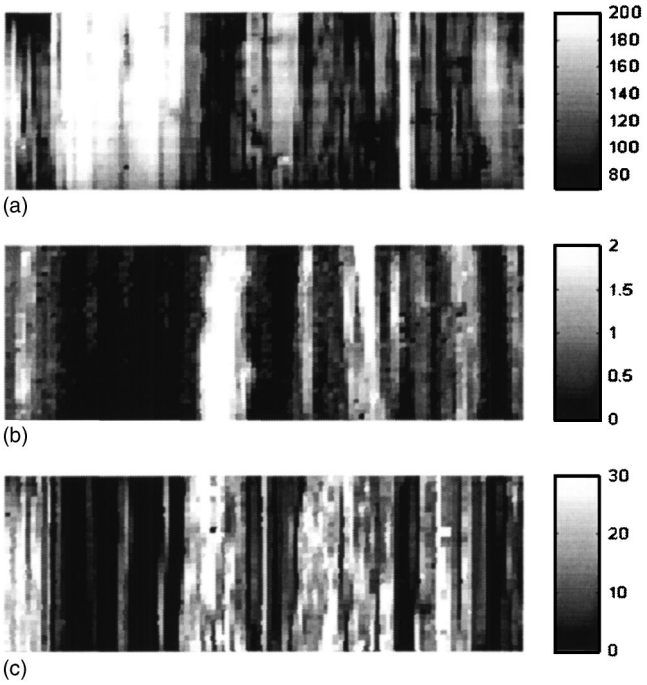

FIG. 8. Room-temperature PL mappings of (a) band-to-band (I_{bb}), (b) defect band (I_{def}), and (c) point-by-point ratio of I_{bb}(hydrogenated)/I_{bb}(initial) representing lifetime upgrade effect. The mapping size is 50×22 mm^2, step $=0.5$ mm.

are the primary carrier recombination center. In addition, the R parameter [R(hydrogenated)] is appreciable in those highly defective regions even after the 750 °C/1 s hydrogenation, indicating that all defects are not fully passivated. Finally, the R parameter increases dramatically in the defective regions after the 700 °C/1 s anneal [R(hydrogenated) vs R(dehydrogenated)], clearly indicating that significant defect dehydrogenation takes place in the area with high defect density. This is further supported by the increase in average R, which is proportional to the active defect concentration, from 0.0111 to 0.0237 after the 700 °C/1 s dehydrogenation (Table II). Figure 9 shows that the reduction in the effective lifetime [I_{bb}(dehydrogenated)/I_{bb}(hydrogenated)], which is

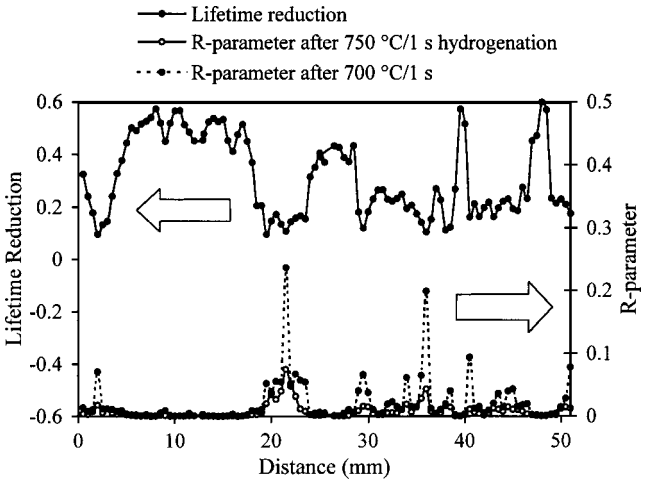

FIG. 9. Line scan through a PL map to quantify loss of carrier lifetime [I_{bb}(hydrogenated)/I_{bb}(dehydrogenated)] and R parameters (I_{def}/I_{bb}) changes after hydrogenation and 700 °C/1 s dehydrogenation.

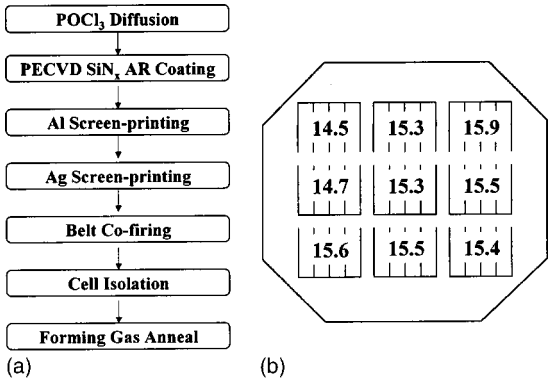

FIG. 10. (a) Process sequence of belt-line cofiring used in this experiment and (b) efficiency distribution of EFG Si solar cells.

caused by the increase in nonradiative recombination centers, seems to be concurrent with the increase in radiative recombination centers or R. This is also supported by the inverse contrast between I_{bb} and I_{def}. Since I_{bb} increases as τ_{eff} increases [Eq. (10)], and τ_{eff} is dominated by the nonradiative recombination centers in Si, the concentration of nonradiative defects decreases with the increase in I_{bb}. Also, the PL intensity of I_{def} decreases with the increase in I_{bb} or τ_{eff} so as τ_{SRH} must increase [Eq. (11)]. The τ_{SRH} represents the radiative component of recombination centers, so the concentration of radiative defects also seems to decrease with the increase in I_{bb}. Thus, dehydrogenation takes place concurrently from both radiative and nonradiative recombination defects, which is supported by the concurrent decrease in I_{bb} and increase in R.

D. Development of a manufacturable belt co-firing process for maximum hydrogenation in EFG Si

Figure 1 shows that the optimum hydrogenation cycle of 775 °C/1 s gave an average EFG Si cell efficiency of 15.3% with a maximum of 15.9%. However, this process involved the two-step RTP firing where the hydrogen passivation of defects was performed at 775 °C for 1 s and the Ag grid contacts were fired at 700 °C for 1 s to avoid contact shunting. Since conventional belt furnace firing is preferred in the PV industry because of high throughput and continuous processing, attempts were made to tailor the temperature profile in a belt furnace to come close to the RTP hydrogenation temperature profile, which can provide effective hydrogenation along with effective Al-BSF formation and good-quality Ag grid contacts in a single firing step. This co-firing process scheme is shown in Fig. 10(a). To avoid contact shunting in the single-step firing scheme, without sacrificing significant hydrogenation, the hydrogenation temperature had to be lowered slightly, and an appropriate Ag paste was selected, which could be fired up to 750 °C without contact shunting. This allowed us to hydrogenate the defects effectively by rapid co-firing of contacts in a belt-line furnace, where peak temperature reached ~750 °C for a very short time. This co-firing process produced a maximum efficiency of 15.9% with an average of 15.1% based on 103 screen-printed EFG

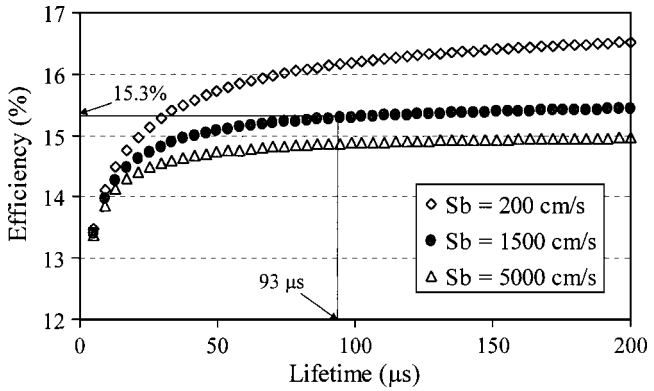

FIG. 11. Model calculation results showing the efficiency and carrier lifetime corresponding with the effective BSRV.

Si cells. Figure 10(b) shows the efficiency distribution of nine 4-cm^2 EFG Si cells on a 100-cm^2 EFG Si wafer.

E. Analysis of loss mechanisms and guidelines for achieving 17% EFG Si solar cells

Model calculations were performed using a one-dimensional modeling software (known as PC1D) to determine the performance-limiting factors and provide guidelines for higher-efficiency EFG Si solar cells. Figure 11 shows the results of model calculations indicating the effect of back surface recombination velocity (BSRV) on screen-printed Si solar cells for this cell design. Table III shows the input parameters used for these calculations. Model calculations revealed that an average efficiency of 15.3% with an average carrier lifetime of 93 μs, achieved in this study for the screen-printed EFG Si cells, corresponds to an effective BSRV value of 1500 cm/s. This is an effective BSRV value because the BSRV may not be spatially uniform because of the inhomogeneous quality of EFG Si. Such a high effective BSRV explains the low average V_{OC} of 600 mV and is also consistent with the high BSRV values reported in Refs. 3 and 23. However, lower V_{OC} could also be the result of inhomogeneity in the bulk lifetime because V_{OC} in the bad region can decay the V_{OC} of the good region.

Model calculations in Fig. 11 also show that ~0.8% enhancement in absolute cell efficiency is possible by reducing the effective BSRV value from 1500 to 200 cm/s on 3.0 Ω cm material. In addition, the introduction of lightly doped emitter and isotropic texturing can raise the screen-printed EFG Si cell efficiency to ~17%.

TABLE III. Material and device parameters used for screen-printed cell simulation.

Parameters	Values
Resistivity	3.0 Ω cm
Thickness	300 μm
Sheet resistance	45.0 Ω/sq
R_s	0.9 Ω cm^2
R_{sh}	10 000 Ω cm^2
J_{02}	5.0 nA/cm^2
Front SRV[a]	35 000 cm/s
Back SRV[a] (S_b)	Variable
SiN_x AR coating	780 Å, index=2.0
Ag grid coverage	7%

[a]SRV-surface recombination velocity.

IV. CONCLUSION

Simultaneous firing of SiN_x at the front and Al at the back of an EFG Si wafer at an optimum temperature for only 1 s raised its carrier lifetime from 3 to >80 μs. This is the result of very rapid SiN_x-induced hydrogenation of defects in EFG Si. A 700 °C/1 s anneal in the absence of a hydrogen supply (SiN_x removed) lowered the carrier lifetime of a hydrogenated EFG sample from 99 to 8 μs because of the rapid dissociation of hydrogen-defect complexes. Therefore, the optimum hydrogenation temperature and the degree of passivation are dictated by the competition between the supply of hydrogen and dissociation of hydrogen-defect complexes during the hydrogenation cycle. The activation energy for hydrogen-defect dissociation was found to be 2.4–2.6 eV, which falls between the activation energies for the dissociation of hydrogen-impurity and hydrogen-dislocation complexes, suggesting the hydrogenation of impurity-decorated dislocations in EFG Si. This was also supported by a defect band observed at 0.8 eV below the conduction band in the PL spectra. Scanning PL spectroscopy clearly showed that defective or low carrier lifetime regions are strongly passivated during the hydrogenation anneal and the same regions are reactivated rapidly during the dehydrogenation anneal.

The optimum hydrogenation anneal produced screen-printed EFG Si solar cells with a maximum efficiency of 15.9% and area-averaged carrier lifetime of ~90 μs. Modeling and analysis of these cells revealed high effective BSRV of 1500 cm/s in the EFG Si cells, neglecting the effect of inhomogeneity in the bulk lifetime on V_{OC}. A reduction of this effective BSRV to 200 cm/s, in conjunction with lifetime enhancement to ⩾200μs, can improve the EFG Si cell efficiency close to 17%.

ACKNOWLEDGMENTS

The authors would like to thank B. R. Bathey at RWE Schott Solar, Inc. for material supply and helpful discussions and D. C. Sutter and B. C. Rounsaville at UCEP for help with SiN_x deposition. This work was supported in part by U.S. DOE (Contract No. DE-FC36-00GO10600) and NREL (Contract Nos. AAT-2-31605-02 and ACQ-9-29639-03).

[1]R. O. Bell and J. P. Kalejs, J. Mater. Res. **13**, 2732 (1998).
[2]J. Jeong, A. Rohatgi, M. D. Rosenblum, and J. P. Kalejs, Proceedings of 28th IEEE Photovoltaic Specialists Conference, Anchorage, AK, 2000, p. 83.
[3]J. Jeong, Y. H. Cho, A. Rohatgi, M. D. Rosenblum, B. R. Bathey, and J. P. Kalejs, Proceedings of 29th IEEE Photovoltaic Specialists Conference, New Orleans, LA, 2002 (unpublished), p. 250.
[4]F. Duerinckx and J. Szlufcik, Sol. Energy Mater. Sol. Cells **72**, 231 (2002).
[5]A. Rohatgi, V. Yelundur, J. Jeong, A. Ebong, M. D. Rosenblum, and J. I. Hanoka, Sol. Energy Mater. Sol. Cells **72**, 117 (2002).
[6]V. Yelundur, A. Rohatgi, A. Ebong, A. M. Gabor, J. I. Hanoka, and R. L. Wallace, J. Electron. Mater. **30**, 526 (2001).
[7]J. Jeong, M. D. Rosenblum, J. P. Kalejs, and A. Rohatgi, J. Appl. Phys. **87**, 7551 (2000).

[8]A. Rohatgi, D. S. Kim, K. Nakayashiki, V. Yelundur, and B. Rounsaville, Appl. Phys. Lett. **84**, 145 (2004).
[9]P. Doshi and A. Rohatgi, IEEE Trans. Electron Devices **45**, 1710 (1998).
[10]A. Rohatgi, S. Narasimha, A. Ebong, and P. Doshi, IEEE Trans. Electron Devices **46**, 1970 (1999).
[11]J. Jeong, A. Rohatgi, V. Yelundur, A. Ebong, M. D. Rosenblum, and J. P. Kalejs, IEEE Trans. Electron Devices **48**, 2836 (2001).
[12]J. P. Kalejs, B. Mackintosh, W. Schmidt, and B. Woesten, Proceedings of 29th IEEE Photovoltaic Specialists Conference, New Orleans, LA, 2002, p. 74.
[13]C. Boehme and G. Lucovsky, J. Vac. Sci. Technol. A **19**, 2622 (2001).
[14]D. Macdonald and A. Cuevas, Appl. Phys. Lett. **74**, 1710 (1999).
[15]P. Atkins, *Physical Chemistry*, 5th ed. (Freeman, San Francisco, 1994), p. 861.
[16]W. L. Hansen, E. E. Haller, and P. L. Luke, IEEE Trans. Nucl. Sci. **NS-29**, 738 (1982).
[17]S. J. Pearton, W. C. Dautremont-Smith, J. Chevallier, C. W. Tu, and K. D. Cummings, J. Appl. Phys. **59**, 2821 (1986).
[18]S. J. Pearton, J. W. Corbett, and T. S. Shi, Appl. Phys. A: Solids Surf. **43**, 153 (1987).
[19]H. J. Möller, *Semiconductors for Solar Cells* (Artech House, MA, 1993), p. 146.
[20]S. J. Pearton (private communication).
[21]S. Ostapenko, I. Tarasov, J. P. Kalejs, C. Haessler, and E.-U. Reisner, Semicond. Sci. Technol. **15**, 840 (2000).
[22]I. Tarasov, S. Ostapenko, W. Seifert, M. Kittler, and J. P. Kalejs, Physica B **308–310**, 1133 (2001).
[23]V. Meemongkolkiat, M. Hilali, K. Nakayashiki, and A. Rohatgi, Technical Digest of 14th International Photovoltaics Science and Engineering Conference, Bangkok, Thailand, 2004, p. 401.